Topographic evolution during deposition of plasma-deposited hydrogenated silicon on glass

G. T. Dalakos*
General Electric Global Research Center, Niskayuna, New York 12309, USA

J. P. Plawsky
Department of Chemical and Biochemical Engineering, Rensselaer Polytechnic Institute, Troy, New York 12180, USA

P. D. Persans
Department of Physics, Applied Physics and Astronomy, Rensselaer Polytechnic Institute, Troy, New York 12180, USA
(Received 28 June 2005; revised manuscript received 19 September 2005; published 3 November 2005)

We report observations of a sequential evolution and morphology of distinct surface morphological growth modes associated with plasma deposition of *a*-Si:H. Each morphology type is associated with a different rate of growth of the surface roughness, ranging from zero to linear. The final steady-state morphology consists of clustered growth, each cluster comprised of similar sized islands, where the clusters grow with time. The limiting size of these islands within each cluster is dictated by island nucleation and surface diffusion rates. Furthermore, nucleation affects the larger-scale morphology, stabilizing the surface by interrupting shadow-induced instabilities. As a result, the rate of surface roughness growth is significantly reduced. Signatures of this mechanism overlap with surface diffusion within the power spectral density function of the topographic data. Surface stabilization by island nucleation has not been reported before for plasma-deposited *a*-Si:H and may be important in surface morphology formation in other growth systems.

DOI: 10.1103/PhysRevB.72.205305 PACS number(s): 68.55.−a, 68.55.Ac

I. INTRODUCTION

Plasma-deposited amorphous hydrogenated silicon (*a*-Si:H) perhaps represents the most-studied material deposited by plasma-CVD techniques. Despite this, the exact mechanism(s) for the observed morphological features on the surface and the evolution of that morphology are not clear. This is especially true for the low temperature data region (<200 °C), as most interest is in higher processing temperatures that are known to produce device quality material for optoelectronic applications.

To describe topographical evolution, we introduce a commonly reported roughness parameter known as the growth exponent.[1] The growth exponent, β quantifies how the surface roughness, or interfacial width changes with time,

$$w(L,t) \sim t^{\beta}, \tag{1}$$

where L is the length scale. At sufficiently long length scales, w is approximately the root-mean-square (rms) roughness.[1] For a two-dimensional surface described by $\mathbf{r}=(x,y)$, the rms roughness is calculated from the relative height data referenced to the mean height, $h(\mathbf{r},t)=z(\mathbf{r},t)-\langle z(\mathbf{r},t)\rangle$,

$$w(L,t) = \sqrt{\langle h(\mathbf{r},t)\rangle}, \tag{2}$$

where the $\langle\cdots\rangle$ term indicates averaging over all points.

If we assemble reported values of β for *a*-Si:H deposition,[2–8] we find a large amount of scatter in the data. This is shown in Fig. 1 showing β as a function of the substrate temperature, T_s. A model explaining the gross temperature dependence of β through most of this data has been proposed by Smets *et al.*[7] The model includes contributions from three distinct growth mechanisms (random growth, surface diffusion, surface relaxation) to explain the change in β with substrate temperature.

With the exception of attempting to explain the temperature dependence of β, multiple growth models describing *a*-Si:H have not been proposed. Instead, a single growth model—the so-called "MGP" model[9–11]—has been widely accepted as the growth model for plasma-deposited *a*-Si:H from silane (SiH_4) feedstock. The MGP model states that SiH_3 film precursors are generated within the plasma region and are later incorporated within the hydrogenated silicon surface through surface dangling bonds—created by a previous abstraction reaction of the surface hydrogen by another SiH_3 radical. Almost complete hydrogen passivation of the surface allows easy diffusion of SiH_3 along the surface and is believed to explain the observed smooth surface topography of *a*-Si:H. Recent studies that have elaborated on the general

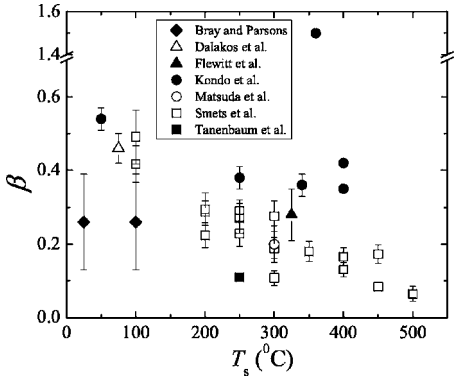

FIG. 1. Reported values of the growth exponent, β for plasma-deposited *a*-Si:H (Refs. 2–8).

 ©2005 The American Physical Society

TABLE I. Processing details of *a*-Si:H deposition.

Sample set	Helium (sccm)	Silane (sccm)	Electrode gap (cm)	RF power (watts)	Pressure (mTorr)
I	1092	6	5.08	200	200
II	392	6	3.81	100	500

MGP model include reactions at strained Si bonds[12] and preferential hydrogen reactions on the *a*-Si:H surface.[4]

If a single set of growth mechanisms for *a*-Si:H does indeed exist, a constant value for β should be observed for the system, independent of processing parameters including T_s. Fractal growth models that include surface diffusion as the primary mass transport mechanism take on different values of β depending on the direction of the incoming flux. For a flux arriving normal to the surface, $\beta=0.25$ results.[1] For an isotropic flux, $\beta=1$ should result at longer deposition times.[13] Reemission models, where the film precursor can reflect off of one surface and land on another can possess β values anywhere from 0 to 1, depending on the sticking coefficient and reemission characteristics.[14,15] Roughening of the surface results from noise in the deposition process as well as shadowing instabilities for non-normal film precursor flux. It is perhaps counterintuitive that β will be constant regardless of the magnitude of the surface diffusivity for both these models.

In real systems, crossover effects may also occur to complicate the process of assigning a single β value to a system. Crossover effects may occur at different times or different length scales and these morphological transitions may be gradual or occur abruptly.[1] A singular value of β may indicate early morphological growth modes and not a system at steady state. Therefore, it is usually necessary to examine the time scale over a few orders of magnitude to rule out or confirm the existence of crossover effects.

II. EXPERIMENT

A. Thin film deposition

A capacitively coupled 13.56 MHz Plasma-Therm 790 deposition/etch system was used to deposit amorphous hydrogenated silicon thin films on Corning 1737F aluminosilicate glass substrates. The substrate was placed on the bottom, grounded electrode (11 in. diameter) within a parallel plate design and heated to 75 °C. Feedstock mixtures of helium and silane were introduced through the top showerhead electrode plate. Immediately before each deposition process, an *in situ* argon plasma sputter cleaning step was used.

We used two sets of processing conditions to deposit *a*-Si:H. Details of these deposition conditions are outlined in Table I. The first set (I) used a low-silane concentration in helium gas mixture (0.42% SiH_4), a system pressure of 200 mTorr, an electrode gap of 5.08 cm and RF input power of 200 W (1.45 W/cm^2). The second set (II) used a higher-silane concentration in helium (2%) at 500 mTorr, a 3.81 cm gap, and 100 W of power. The calculated *a*-Si:H deposition rates determined from ellipsometric measurements, for set I and set II were 12.5 ± 1.0 and 11.6 ± 0.8 nm/min, respectively.

B. Thin film characterization

Surface topographic data was obtained by atomic force microscopy (AFM). Tapping-mode AFM analysis was performed using a Digital Instruments Dimension 3100 Microscope with a Nanoscope IIIa Controller. Two types of tips were used—a standard-sized Tap300 etched Si tips and high-resolution 0.5 nm carbon nanotube tips. The standard is an etched silicon tip with a radius of curvature of approximately 5 nm and 75 kHz resonance frequency and 5 N/m force constant. The smaller radius probe has a 1 nm radius of curvature created from carbon growth on the standard AFM probe described previously. Scanned pixel sizes of 256×256 and 512×512 were used at various scan lengths from $L=250$ to 2000 nm.

Post processing included second order leveling of the data to account for slight system drift during scanning. Data analysis included calculating the rms roughness [Eq. (2)] and the isotropic power spectral density (PSD) function. The PSD is defined as $g(\mathbf{q})=\langle|h(\mathbf{q})|^2\rangle$, where $h(\mathbf{q})$ is the Fourier transform of the image in real space. The AFM software algorithm calculates a one-dimensional isotropic PSD function, defined as $\sim g(\mathbf{q})(2\pi\mathbf{q})^{-1}$, and reported in units of nm^3. Sufficiently long length scales were used to calculate the rms roughness, w (i.e., region where w is not dependent on local length scale).[1]

Long-range order within *a*-Si:H was examined by grazing incidence x-ray diffraction ($\alpha=0.5°$) using a Bruker D8 Advance diffractometer. The instrument uses Cu K_α radiation and is equipped with a thin-film attachment.

Infrared transmission measurements using the Fourier transfer ir (FTIR) technique were used to study silicon hydride bonding within the bulk material. The vibrational modes of interest included a bending and/or scissors mode for dihydride bonding (doublet, 840–890 cm^{-1}), a stretching mode from isolated monohydrides ($\sim$2000 cm^{-1}), and a stretching mode from clustered monohydrides and/or polyhydrides ($\sim$2100 cm^{-1}).[16]

Rutherford backscattering spectrometry (RBS) and nuclear resonance analysis (NRA) were employed to quantify the silicon and hydrogen atomic fractions within the bulk *a*-Si:H material.

III. RESULTS

Upon examination of the surface topography of the films in sets I and II, we discovered three distinct types of morphology. In general, the types of morphology exhibited ex-

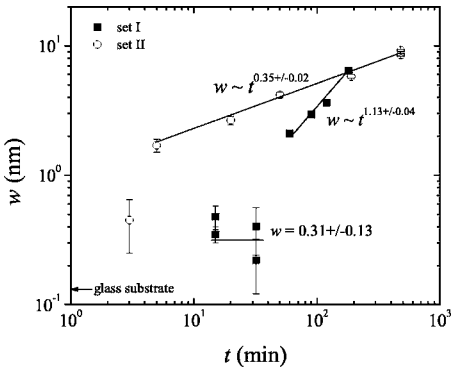

FIG. 2. rms roughness of *a*-Si:H as a function of deposition time.

tensive wavelength selection—ordered features that grew in size and exhibited different length scales. We also found different values of the dynamic scaling coefficient, β associated with the different morphology types.

These multiple β values are shown from the calculated rms roughness values of the two data sets, plotted as a function of time, t in Fig. 2. The rms roughness of the uncoated 1737F glass is also indicated in the figure. Power functions of the form $y=c_1x^{c_2}$, where c_1 and c_2 are constants, were fit to the data; c_2 corresponds to the growth exponent, β.

The films in set I exhibited featureless topography until $t=32$ min; the measured rms roughness is small and apparently independent of t (Fig. 2). The single value of the rms roughness was calculated at 0.31 ± 0.13 nm. No distinct features on the surface could be resolved from either high-resolution SEM or the AFM scans. Nonetheless, we found that these rms roughness values were larger than the rms roughness of the uncoated glass substrate surface of 0.13 ± 0.03 nm indicating that distinct features on the surface may in fact, exist. We assign a $\beta\sim0$ for this region, although an upper limit may be more suitable for the initial growth mode.

After $t=32$ min, the morphology consist of an ordered hillock formation whose size increases with t as shown in the AFM images of Fig. 3. A distinct peak in the isotropic PSD function (Fig. 4) indicates mounded morphology. The PSD spectra shows a shift in the peak to smaller wave vectors and a decrease in the full-width-half-maximum (FWHM) value with t. The spectra exhibits a $\mathbf{q}^{-4}$ dependence at shorter length scales (higher wave vectors). The rms roughness grows at approximately a linear rate ($\beta=1.13\pm0.04$ from $t=32-180$ min) during this mounded growth region as shown in Fig. 2.

The samples in set II also exhibit initial smooth layer formation followed by mounded island growth as in set I. The crossover between these two morphological types however, occurs at much earlier times. Featureless morphology from set II films was maintained up to a thickness of ~30 nm as evident from SEM cross sections (compare with the crossover from set I films at ~200 nm). After this thickness is reached, periodic feature morphology on the surface starts to appear. This is seen in the AFM scan at $t=3$ min (thickness of ~35 nm) in Fig. 5. With time, the morphology takes on the form of growing clusters made up of constant-sized islands. Island upon island-type morphology (i.e., cluster formation) is not observed in set I films under the time scales examined. The measured island size and the cluster domain size (approximately equal to the correlation length within the PSD function) from AFM scans of set II films at different processing times is shown in Fig. 6. Growth of the individual islands quickly reach a maximum diameter of 24.8 ± 2.3 nm. This is based on AFM measurements using a 2–5 nm Si tip. Because the tip size is close to the value of the feature sizes, the actual value will be somewhat smaller. A rescanned image of the samples at $t=90$ min using a smaller sized tip (0.5 nm) yielded a smaller value for the island feature length of 17.4 ± 2.4 nm.

We calculate a $\beta=0.35\pm0.02$ value from $t=5$ to 480 min associated with clustered-island topography. As with set I, the PSD functions from set II exhibit $\mathbf{q}^{-4}$ scaling at higher $\mathbf{q}$, but do not show prominent peaks within the functions.

Material properties

The deposited films were determined to be amorphous from the absence of diffraction peaks in the XRD spectrum. The main differences discovered between the two sets of data (I and II) was the bulk hydrogen content and the hydrogen's bonding configuration.

Examination of ir transmission spectra indicate a noticeable difference in the silicon hydride bonding configurations between the two processing conditions. The calculated absorption coefficient is obtained from the method described by Langford *et al.*[16] and plotted in Fig. 7. The calculated absorption coefficient, α is normalized by the frequency, ν, where both are in units of cm^{-1}. The set I material shows a stronger response from the ($Si-H_2$) bending or scissors vibrational mode shown by doublet absorption peaks at 840–890 cm^{-1}. A larger 2100/2000 peak ratio for set I also indicates a higher dihydride to monohydride ratio. The total hydrogen content of the films can be estimated from the two Si-H bending modes at 2000 and 2100 cm^{-1} as described by Langford *et al.*[16] Assuming the bulk silicon density of 5×10^{22} cm^{-3}, we obtain a 20% and 26% total hydrogen content for sets I and II films, respectively.

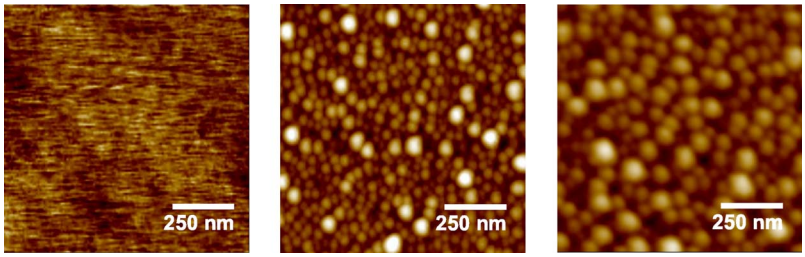

FIG. 3. (Color online) Top-down AFM scanned images ($L=1\times1$ μm) from set I films at various deposition times. Deposition times and the height range (Δz) are listed under the image.

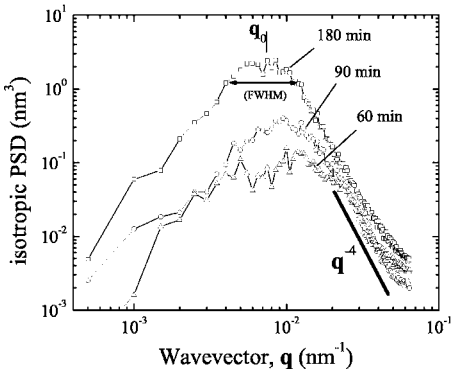

FIG. 4. The isotropic PSD function of the set I surfaces at t =60, 120, and 180 min.

From RBS/NRA analysis, the films in set I had a lower density (1.6 to 2.1 g/cm^3) and a higher atomic hydrogen to silicon ratio compared to films from set II. The atomic composition was determined to be $SiH_{0.7}$ or 41% hydrogen (set I) and $SiH_{0.35}$ or 25% hydrogen (set II).

IV. DISCUSSION

The observed morphology associated with a-Si:H and it's temporal behavior is quite complex. However, some main features of how this morphology evolves can be explained by simple assumptions regarding the nature of the flux and the movement of film precursors along the surface.

In vapor deposition by CVD and sputtering at low temperatures (i.e., conditions occurring far from thermodynamic equilibrium), evolution of the deposited film topography occurs from competitive mechanisms between stochastic noise and/or shadowing instability and limited surface diffusion.[17] Shadowing effects arise from the non-normal incident flux of film precursors. Loosely bound surface adatoms will be the only species that can participate in mass transport on the surface at these relatively low temperatures (i.e., surface relaxation and viscous flow rates are relatively slow at these temperatures[18]).

A simple model of the surface height profile $[h(\mathbf{r},t)]$ describing thin film morphology evolution under these conditions has been previously applied to sputtering.[17] The model

$$\frac{dh}{dt} = -K\nabla^4 h + F\theta(\mathbf{r},\{h\}) + \eta(\mathbf{r},t), \tag{3}$$

includes terms that capture smoothing by curvature-driven surface diffusion[19] $(-K\nabla^4 h)$ and roughening via a shadowing instability $[F\theta(\mathbf{r},\{h\})]$. $\eta(\mathbf{r},t)$ accounts for random noise from the incoming flux. K is proportional to the diffusion coefficient, F is the interface velocity normal to the surface, and θ is the exposure angle to the incoming flux.

The solution to the linear version of Eq. (3) yields the isotropic power spectral density function

$$g(\mathbf{q},t) = \langle |h(\mathbf{q},t)|^2 \rangle = \Omega \frac{1 - \exp[-2(K\mathbf{q}^4 - F\mathbf{q})t]}{2(K\mathbf{q}^4 - F\mathbf{q})}, \tag{4}$$

where $h(\mathbf{q},t)$ is the radially averaged Fourier transform of $h(\mathbf{r},t)$ and Ω is proportional to the incoming flux. The diffusion term influences $g(\mathbf{q},t)$ at larger values of $\mathbf{q}$, smoothing out shorter length scales and associated with a $\mathbf{q}^{-4}$ scaling.

The calculated isotropic PSD function, $g(\mathbf{q},t)$ in Eq. (4), exhibits characteristics found in the measured isotropic PSD functions of set I as shown in Fig. 8. The inset shows set I PSD functions from Fig. 4. The model correctly predicts an increase in the magnitude and shifting of the peak $(\mathbf{q}_c)$ to smaller $\mathbf{q}$ and a reduction of the FWHM as t increases.[20] The decrease in the measured PSD curves at smaller wave vectors is not predicted by the continuum equation. Here $g(\mathbf{q})$ consists of random noise only. The discrepancy at shorter wave vectors might be due to wavelength-dependent noise sources.

This model describing mounded growth quite well does not take into account the island nucleation associated with set II films. Island nucleation has been reported as a stabilizing mechanism in epitaxial growth based on numerical simulations[21] and observed from experimental results.[22] It is indicated by a $\mathbf{q}^{-4}$ scaling within the isotropic PSD function. Coincidentally, the same scaling magnitude is associated with surface diffusion smoothing. Careful examination of images of the surface and feature sizes do in fact indicate that nucleation is captured in the PSD function—although it is easy to overlook.

From the PSD functions of set II films we observe that island nucleation appears to stabilize mounded morphology stochastically—the prominent peaks found in set I PSD functions are not present in the set II PSD functions, but instead are suppressed as shown in Fig. 9. At t=3 min, just before clustered island domains can form (Fig. 5), we see a small but defined peak within the PSD function as indicated in the figure. This peak reflects ordered mounded structures on the surface, caused by nonstochastic shadowing of surface perturbations. Suppression of these instabilities and the peak is shown at later times at t=45 min. The PSD function exhibits scaling behavior $\mathbf{q}^{-4}$, corresponding to surface diffusion and island nucleation stabilizing mechanisms.

While the two stabilizing mechanisms share the same $\mathbf{q}^{-4}$ scaling, we may differentiate between the two simply by

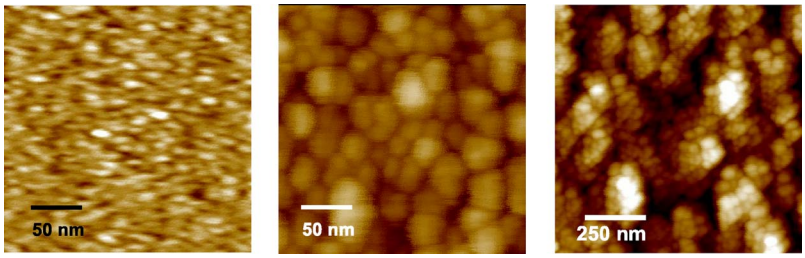

FIG. 5. (Color online) Top-down AFM scanned images from set II films at various deposition times. Height range (Δz) and scan lengths, L are listed under the image.

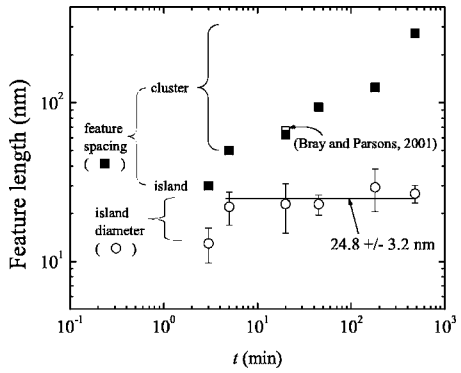

FIG. 6. Length scales of island and cluster domains from set II films. Reported correlation length at $t=20$ min for films deposited at $T_s=75$ °C by Bray and Parsons is also shown (Ref. 2).

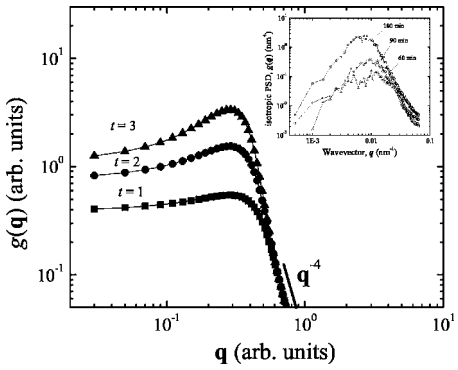

FIG. 8. Calculated $g(\mathbf{q},t)$ shown with the isotropic-PSD functions from set I (plot inset). The parameters used to calculate $g(\mathbf{q},t)$ include $\Omega=0.2$, $K=20$, and $F=1.5$.

noting the various feature sizes. Figure 10 shows an AFM scan (inset) and PSD function of the set II sample at $t=45$ min using the smaller AFM 0.5 nm tips. The PSD function shows a $\mathbf{q}^{-4}$ scaling of frequency ranges corresponding to the average island size and cluster size. The approximate length scale, L_c separating these two regions is shown in the image inset and PSD function. Higher frequencies $\mathbf{q}$ than $2\pi/L_c$ correspond to surface diffusion. Lower frequencies up to corresponding cluster sizes are stabilized by island nucleation.

It is clear then that surface diffusion acts as the smoothing mechanism at island-sized length scales of whose maximum diffusion length will be influenced by new island nucleation. The average diffusion length of SiH_3 on the a-Si:H is approximated by $\Lambda=\sqrt{D\tau}$, where D is the diffusion coefficient and τ is the lifetime of SiH_3. While both D and τ could be changing under different processing conditions, variability in D is usually only associated with substrate temperature T_s. Therefore, the adatom lifetime, τ would likely determine the different diffusion length scales observed in sets I and II.

Recent studies of surface diffusion of SiH_3 indicate that it is surface reaction limited,[23] and dependent on local curvature (i.e., valleys and peaks) and dangling bonds.[24] The lifetime of a physisorbed SiH_3 is short compared to the SiH_3 arrival, $\sim 2\ s^{-1}$ adatom per 10 Å^2 surface site area is calculated from our deposition rate. Desorption of the adatom back into the gas phase is not likely to occur based upon it's large associated threshold energy of 0.7 eV.[25] Therefore, major pathways for the adatom's fate include either film incorporation or hydrogen abstraction. The latter reaction forming stable $SiH_4(g)$. The likely SiH_3 incorporation pathway is it's reaction with strained[12] or dangling bonds.[25]

An expression relating the surface reaction-limited diffusion length has been previously derived,[25,26]

$$\Lambda = \left(\frac{\nu_h}{2\nu_a} \frac{a^2}{\left(1+\frac{\nu_b}{\phi}\right)} \right)^{1/2}, \tag{5}$$

where a^2 is the reaction site area (~ 10 Å^2), ν is the reaction rates for abstraction (a), adatom hopping (h), and hydrogen desorption (b). ϕ is the adatom flux to the surface. At low T_s we may neglect hydrogen desorption (i.e., $\nu_b \ll \nu_a, \nu_h$) due to a relatively high associated threshold energy of $E_d=2.1$ eV.[27] Equation (5) can then be simplified to

$$\Lambda = (a^2/2\theta_0)^{1/2}, \tag{6}$$

where $\theta_0 \equiv \nu_a/\nu_h$ is simply the dangling bond concentration on the surface.

According to the above equations, the length scale differences observed in sets I and II will be due to differences in

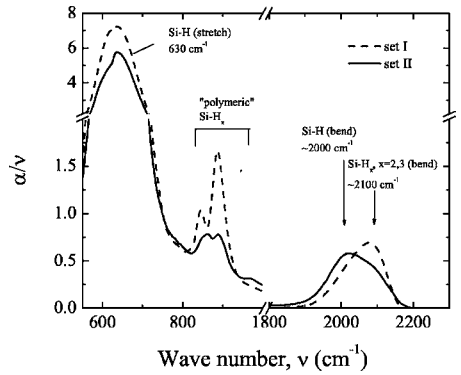

FIG. 7. Optical absorption in the ir region ($\nu=4000$ to 550 cm^{-1} wave numbers) attributed to silicon hydride (SiH_x, $x=1,2,3$) vibrational modes.

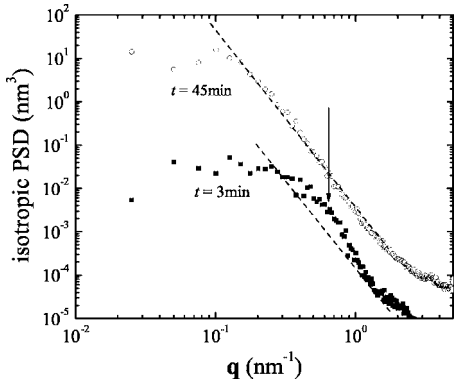

FIG. 9. Isotropic PSD functions of set II sample at $t=3$ min and $t=45$ min. The dotted line indicates a $\mathbf{q}^{-4}$ scaling. A peak in the PSD function at $t=3$ min is indicated in the figure.

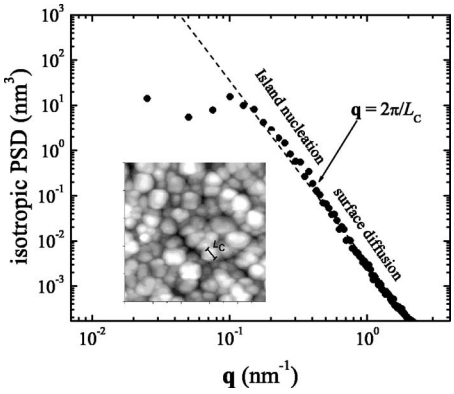

FIG. 10. PSD function with image inset ($L=250\times250$ nm) of set II at $t=45$ min. The approximate feature size, L_C differentiating island nucleation and surface diffusion is indicated.

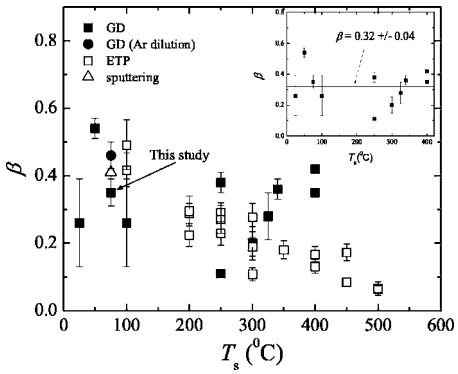

FIG. 11. Replotted data from Fig. 1 as a function of deposition method including the measured steady-state set II β value. The plot inset is glow discharge data suggesting temperature independence with $\beta=0.3\pm0.04$.

dangling bond surface concentrations. We do not know the surface dangling bond concentrations of the two films sets but we know that they possess different hydrogen contents and bonding arrangements from RBS and FTIR measurements. We find that the films in set I possess a higher hydrogen content and higher concentration of dihydride bonds relative to the set II films. If the concentration of dangling bonds is inversely proportional to a higher hydrogen content, the higher hydrogen content film would exhibit longer length scales as shown in set I. This assumption is consistent with growth models[25] that predict smaller diffusion lengths with larger concentration of dangling bonds as T_s increases—as well as a simultaneous decrease in hydrogen within the bulk material. It is thus anticipated that high island nucleation rates would result from a surface possessing a high concentration of dangling bonds.

It is reasonable to suggest that at sufficiently long time scales, the morphology from set I would result in island nucleation, similar to set II. Details of the surface kinetics—possibly the dangling bond concentration—would provide insight into the critical length scales of the system. Longer depositions under set I conditions would be needed to verify this.

The multiple changes in processing conditions (silane concentration, pressure, electrode gap) for the two sets make simple predictions into mechanistic differences (plasma, surface kinetics), difficult. From the similar deposition rates of the two conditions, the flux of film precursor species is also assumed to be similar. This would also support the idea that diffusion length is surface reaction limited and not terminated because of the adatom flux (i.e., dimer island formation, burial of adatoms by arriving atoms). Thus surface differences, such as dangling bond concentrations would explain morphological length and time scales for the observed differences of the two sets.

We may extend this reasoning to other conditions of interest such as higher deposition temperatures—processing conditions that are favored for device fabrication. Despite the highly dependent nature of reaction rates on temperatures, island nucleation may not be as sensitive as anticipated. Higher deposition temperatures are expected to result in an increase in the dangling bond concentration and/or decrease in hydrogen concentration. This would be expected to translate in an increase in nucleation rate and decrease in the adatom lifetime. The affects of the reduced adatom lifetime, τ on the final diffusion length, λ would be offset by an increase in the diffusion coefficient, D following an Arrhenius temperature dependence.

An unusual observation of initial featureless morphology for both processing conditions may be due to surface energy modification of the uncoated glass. We have not explored this phenomena in depth but note it's occurrence when in the presence of the initial argon etch step—elimination of the etch step was seen to result in immediate onset of surface roughening without initial smooth layer formation.[28,29] We have previously reported smooth topography under cathodic deposition[30] (i.e., conditions under energetic ion-assisted growth) also at $T=75$ °C, resulting in $\beta\sim0$. The reason why this occurs or if it relates to low β values of anodic a-Si:H deposited at higher T_s (see Fig. 1) is unknown.

From this study, we have observed three distinct β values for a-Si:H deposition at $T_s=75$ °C spanning from $\beta\sim0$ to ~1. It is perhaps not surprising then that historic β measurements have shown a large scatter making it very difficult to assess the true value of it. If we consider all β values from the two data sets, the one that appears to be most relevant is the one describing the steady state value from set II. At these times, clustering has occurred and a constant island size has been established. This is when $\beta=0.35\pm0.02$. This value does not correspond to standard models describing a self-affine surface,[1] but may be a result of the complicated interaction of mass transport mechanisms such as surface diffusion, shadowing, surface reflection, and surface reactions.

If we compare this value with other reported β values using glow discharge (GD) techniques, we find that our value roughly agrees with the previous data and suggests a constant temperature-independent β value. Figure 11 replots Fig. 1 as a function of deposition technique, including our calculated, steady-state value of β. Assuming a slope of zero, a $\beta=0.3\pm0.04$ is calculated from the GD data set (the calculated value excludes the outlying Kondo data point of $\beta\sim1.5$) and shown as the Fig. 11 inset plot. Temperature independence of the β value would be consistent with a single a-Si:H deposition model. The lower values of β, occurring

at $T_s > \sim 300\,^{\circ}\mathrm{C}$ may indicate a change in the surface growth model. This could involve the onset of H_2 evolution from Si-H bond rearrangement[25] that occurs at higher T_s or surface relaxation as Smets *et al.* have suggested.[7]

The large scatter in the data underscores the difficulty of describing the complex morphology with a single parameter (β). It also may be a reflection of crossover effects and unsaturated β values causing the large scatter within the data.

In summary, we find that the temporal nature of surface morphology evolution of *a*-Si:H progresses though a sequence of distinct modes. Associated with each one of these modes is a certain rate of growth of the surface roughness. The differences in the rate are large and quite noticeable, ranging from zero for initial smooth, featureless morphology to linear for island shadowed-instability growth. Of most interest is the final mode, that may be viewed as the steady-state mode—at least from the time scales investigated here. This mode consists of clustered growth comprised of similar sized islands. Island nucleation, which stabilizes surface roughness by interrupting shadowing instability has not been reported before for plasma-deposited *a*-Si:H and may be present in many other growth systems as well. This may not be surprising as it's signature in the power spectrum ($\mathbf{q}^{-4}$) exhibits the same scaling as surface diffusion and may be mistaken for it. The competition between surface diffusion versus island nucleation determines the final feature size—assuming similar precursor flux distribution to the surface. In *a*-Si:H, surface diffusion of SiH_3 is affected by a number of factors and is complex. In this study, we have been able to obtain a large difference of feature sizes in two film sets that are believed to derive from their different hydrogen contents. Of course, many more deposition conditions may be explored that can affect the rates of island nucleation and surface diffusion and therefore, the characteristic island sizes and the occurrence of these distinct morphology types in a similar manner.

ACKNOWLEDGMENTS

The authors wish to acknowledge Julie Teetsov (GE) and Rosylin Klinger (GE) for conducting AFM measurements, Yan Gao (GE) for XRD analysis, and Hassa Bakhru (State University of New York, Albany) for RBS measurements. The authors also thank Tansel Karabacak (RPI) for helpful discussions on thin film morphology evolution. GE Global Research is acknowledged for covering the publication costs.

*Electronic address: dalakos@research.ge.com

[1] A. L. Barabasi and H. E. Stanley, *Fractal Concepts of Surface Growth* (Cambridge University Press, Cambridge, 1995).
[2] K. R. Bray and G. N. Parsons, Phys. Rev. B **65**, 035311 (2002).
[3] G. T. Dalakos, J. L. Plawsky, and P. D. Persans, Mater. Res. Soc. Symp. Proc. **715**, A.19.4. (2002).
[4] A. J. Flewitt, J. Robertson, and W. I. Milne, J. Appl. Phys. **85**, 8032 (1999).
[5] M. Kondo, T. Ohe, K. Saito, T. Nishimiya, and A. Matsuda, J. Non-Cryst. Solids **227–230**, 890 (1998).
[6] A. Matsuda, K. Nomoto, Y. Takeuchi, A. Suzuki, A. Yuuki, and J. Perrin, Surf. Sci. **22**, 50 (1990).
[7] A. H. M. Smets, D. C. Schram, and M. C. M. van de Sanden, Mater. Res. Soc. Symp. Proc. **609**, A.7.6.1 (2000).
[8] D. M. Tanenbaum, A. L. Laracuente, and A. Gallagher, Phys. Rev. B **56**, 4243 (1997).
[9] A. Matsuda and K. Tanaka, J. Non-Cryst. Solids **97**, 1367 (1987).
[10] A. Gallagher, J. Appl. Phys. **63**, 2406 (1988).
[11] J. Perrin, J. Non-Cryst. Solids **137**, 639 (1991).
[12] J. R. Abelson, Appl. Phys. A: Solids Surf. **56**, 493 (1993).
[13] J. H. Yao and H. Guo, Phys. Rev. E **47**, 1007 (1993).
[14] Y.-P. Zhao, J. T. Drotar, G.-C. Wang, and T.-M. Lu, Phys. Rev. Lett. **87**, 136102 (2001).
[15] T.-M. Lu, Y.-P. Zhao, J. T. Drotar, T. Karabacak, and G.-C. Wang, Mater. Res. Soc. Symp. Proc. **749**, W1.2.1 (2003).
[16] A. A. Langford, M. L. Fleet, B. P. Nelson, W. A. Lanford, and N. Maley, Phys. Rev. B **45**, 13367 (1992).
[17] R. P. U. Karunasiri, R. Bruinsma, and J. Rudnick, Phys. Rev. Lett. **62**, 788 (1989).
[18] A. Witvrouw and F. Spaepen, J. Appl. Phys. **74**, 7154 (1993).
[19] C. Herring, J. Appl. Phys. **21**, 301 (1950).
[20] Y.-P. Zhao, H.-N. Yang, G.-C. Wang, and T.-M. Lu, Phys. Rev. B **57**, 1922 (1998).
[21] P. Politi and J. Villain, Phys. Rev. B **54**, 5114 (1996).
[22] J. E. Van Nostrand, S. J. Chey, and D. G. Cahill, Phys. Rev. B **57**, 12536 (1998).
[23] S. Ramalingham, S. Sriraman, E. S. Aydil, and D. Maroudas, Appl. Phys. Lett. **78**, 2685 (2001).
[24] M. S. Valipa, S. Sriraman, E. S. Aydil, and D. Maroudas, Surf. Sci. **574**, 123 (2005).
[25] J. Robertson, J. Appl. Phys. **87**, 2608 (2000).
[26] J. Perrin, M. Shiratani, P. Kae-Nune, J. Jolly, and J. Guillon, J. Vac. Sci. Technol. A **16**, 278 (1998).
[27] J. E. Northrup, Phys. Rev. B **44**, R1419 (1991).
[28] In epitaxial growth, layer-by-layer mode growth occurs when $\gamma_A < \gamma_B + \gamma^*$, where γ_B is the substrate surface energy, γ_A is the surface energy of the film, and γ^* is the interfacial energy, defined as the excess energy over the bulk film and substrate, integrated over the interfacial region (Ref. 29).
[29] J. A. Venables, *Introduction to Surface and Thin Film Processes* (Cambridge University Press, Cambridge, 2000), p. 147.
[30] G. T. Dalakos, J. L. Plawsky, and P. D. Persans, Appl. Phys. Lett. **85**, 3462 (2004).